

Application of wavelength-scanned wavelength-modulation spectroscopy H_2O absorption measurements in an engineering-scale high-pressure coal gasifier

Kai Sun · Ritobrata Sur · Jay B. Jeffries ·
Ronald K. Hanson · Tommy Clark ·
Justin Anthony · Scott Machovec · John Northington

Received: 29 August 2013 / Accepted: 19 April 2014 / Published online: 6 May 2014
© Springer-Verlag Berlin Heidelberg 2014

Abstract A real-time, in situ water vapor (H_2O) sensor using a tunable diode laser near 1,352 nm was developed to continuously monitor water vapor in the synthesis gas of an engineering-scale high-pressure coal gasifier. Wavelength-scanned wavelength-modulation spectroscopy with second harmonic detection (WMS-2f) was used to determine the absorption magnitude. The 1f-normalized, WMS-2f signal (WMS-2f/1f) was insensitive to non-absorption transmission losses including beam steering and light scattering by the particulate in the synthesis gas. A fitting strategy was used to simultaneously determine the water vapor mole fraction and the collisional-broadening width of the transition from the scanned 1f-normalized WMS-2f waveform at pressures up to 15 atm, which can be used for large absorbance values. This strategy is analogous to the fitting strategy for wavelength-scanned direct absorption measurements. In a test campaign at the US National Carbon Capture Center, the sensor demonstrated a water vapor detection limit of ~ 800 ppm (25 Hz bandwidth) at conditions with more than 99.99 % non-absorption transmission losses. Successful unattended monitoring was demonstrated over a 435 h period. Strong correlations between the sensor measurements and transient gasifier operation conditions were observed, demonstrating the

capability of laser absorption to monitor the gasification process.

1 Introduction

In modern energy systems [1], there is a need for sensors to rapidly monitor the gas composition, providing control signals to optimize the system performance for increased energy efficiency and decreased pollutant emissions [2]. For the harsh environment of a coal gasifier in an integrated gasification combined-cycle power plant, safety requirements to handle the hot, high-pressure, toxic and explosive synthesis gas (called here syngas) and fouling by particulate make it difficult to install a gas analyzer directly into the gas flow for in situ measurements. Thus, most sensors rely on gas sampling measurements, which produce time delays and slow time resolution (minutes). In addition, although H_2O is a major combustion product, many sampling-based gas analyzers such as gas chromatography (GC) require removing the water vapor before the analysis. As a result, rapid real-time H_2O monitoring data are unavailable in most industrial systems.

Wavelength-modulation absorption spectroscopy (WMS) using injection-current-tuned diode lasers (TDL) has been employed for more than a decade for in situ sensors to determine gas composition, temperature, pressure and velocity in a variety of harsh industrial environments and laboratory combustors [3–12], and commercial instruments using WMS have been available for a decade [13, 14]. Compared to direct absorption (DA) measurements, WMS can improve the signal-to-noise ratio (SNR) [15–17], avoid the need to measure a zero-absorption baseline during data collection [18, 19] and be less influenced by non-absorption transmission losses [11, 12, 20,

K. Sun (✉) · R. Sur · J. B. Jeffries · R. K. Hanson
High Temperature Gasdynamics Laboratory, Stanford
University, Stanford, CA 94301, USA
e-mail: hermitford@gmail.com

J. B. Jeffries
e-mail: Jay.Jeffries@Stanford.edu

T. Clark · J. Anthony · S. Machovec · J. Northington
National Carbon Capture Center, Southern Company Services,
Wilsonville, AL 35186, USA

21]. These WMS features have proven useful for sensors in practical industrial applications, especially for applications with large and time-varying non-absorption transmission losses [21–25]. Although an attempt to review the use of WMS for in situ measurements in practical applications is beyond the scope of this paper, two pioneering applications of $1f$ -normalized, wavelength-scanned WMS- $2f$ were performed previously in harsh environments [11, 12]. Fernholz et al. [11] demonstrated $1f$ -normalized wavelength-scanned WMS of oxygen in the exhaust from a high-pressure (12 atm) flame, and a 1998 meeting report from the same group discussed the use of this method for measurements of O_2 in the effluent of a 20 MW_{th} hazardous waste incinerator [12]. Although the wavelength-scanned WMS sensor architecture and $1f$ -normalization of the signal are quite similar to this past work, our new data analysis method is quite different. The pioneering work in Refs. [11] and [12] accounted for simultaneous amplitude modulation during the scan of the laser wavelength; however, this earlier method did not account for nonlinear response of the laser tuning and was limited to measurements of small absorbance.

Here, we report application of $1f$ -normalized, wavelength-scanned WMS- $2f$ to a high-pressure (15 atm) synthesis gas product stream with large non-absorption transmission losses, using a newly developed analysis scheme [26, 27] that allows fits of the wavelength-scanned WMS signal waveform to an absorption spectrum similar to wavelength-scanned direct absorption. Importantly, this new method is not limited to optically thin conditions and can account for nonlinearity in the laser modulation. Because this is the first application of the wavelength-scanned WMS method of Refs. [26] and [27] to increased pressure gases, we also present gas cell measurements taken with known conditions at pressures from 3 to 15.8 atm.

Laser absorption measurements in syngas products from coal gasification have two major challenges: high pressures broaden and blend the laser absorption transitions, and the scattering from particulate in the gas significantly attenuates the transmitted laser intensity. In previous work, we found that $1f$ -normalized, fixed-wavelength WMS provided a solution to these challenges, and the composition and temperature of syngas products were monitored in a pilot-scale entrained-flow high-pressure coal gasifier [28–30].

In this paper, the sensor performance was improved through the use of wavelength scanning and a new paradigm for WMS data reduction, and this improved sensor was used for long-term monitoring of the water vapor in the syngas output from a significantly larger (engineering-scale) high-pressure transport reactor facility. Compared to the fixed-wavelength WMS technique used for our earlier gasifier applications, the wavelength-scanned WMS

technique is less affected by drifts in the laser wavelength or pressure shifts in the absorption transition center wavelength. In addition, wavelength-scanned WMS simultaneously determines the WMS absorption lineshape and thus minimizes the errors due to the variations of the transition's collisional width caused by changes in gas composition. Thus, the wavelength-scanned WMS approach demonstrated in this paper is more suitable for long-term (days) monitoring in complex gas flows, where the laser wavelength may shift and variations in the collisional width of the absorption transition due to changes in the gas composition are hard to estimate.

The wavelength-scanned WMS data analysis scheme recently developed in our laboratory [26, 27] fits each wavelength scan of the $1f$ -normalized WMS- $2f$ absorption waveform while varying only the integrated absorbance and the width of the lineshape of the target transition. All other laser scanning and performance parameters are fixed from characterization measurements [22, 23] in the laboratory before (and verified after) the field campaign. The use of $1f$ -normalization and laser characterization [22, 23] avoids the need for in situ sensor calibration often required for WMS sensors and was termed “calibration-free” in Ref. [23]. We have found that the laser characterization parameters for near-infrared telecommunications lasers (NEL used here) have remained constant over several years of regular use in our laboratory and in the field. Even so, these parameters are verified before and after any measurement campaign. Obtaining a fit value for the transition linewidth accounts for any changes in the gas composition without the need for a large database of collision-broadening parameters (this assertion is tested as described below by comparison with the linewidth determined from a collision-broadening database and independently gas composition measurements with the linewidth determined by the wavelength-scanned WMS fits from the TDL sensor data). The normalization scheme [11, 12, 23] accounts for losses in transmission that is independent of laser wavelength over the region of the scan (e.g., time-varying scattering losses) as well as providing a signal independent of detector gain. Here, the goal is to present the results using this new scheme for in situ monitoring of water vapor in syngas products from a nearly commercial-scale gasifier, and the reader should refer to Refs. [26] and [27] for the details of the data analysis scheme.

Before assembling a prototype sensor for the NCCC field measurement, the sensor performance was investigated at increased pressures by measuring the wavelength-scanned WMS of water vapor in a laboratory cell using a DFB laser (NEL) near 1,352 nm. The integrated absorbance and collisional width of the probed transition was simultaneously determined, over a pressure range from 3 to 15.8 atm and compared with expected values. The TDL

sensor was then packaged and used for in situ measurements in the syngas in an engineering-scale transport reactor high-pressure coal gasifier at the National Carbon Capture Center [31]. The prototype sensor was used for continuous monitoring of the water vapor content in the output syngas for more than 27 days.

2 Wavelength-scanned WMS method

The analysis used here for the injection-current-tuned wavelength-scanned WMS measurements has been published previously [26, 27]. Here, we only review the key steps used to simulate the WMS-*nf* absorption signals to guide the discussion. For consistency with these earlier reports, the concept of a zero-absorption transmitted laser intensity, $I_{bg}(t)$, is introduced; however, for practical industrial applications, this intensity cannot be measured, and other strategies to determine this quantity are described in the section below on the field measurements.

For typical wavelength-scanned measurements (see Fig. 1), the laser wavelength is modulated rapidly by varying its injection current at frequency f superimposed upon a slow scan of the mean injection current of the modulated laser at frequency f_s . The laser wavelength and intensity are simultaneously modulated and ramped by this variation of injection current.

The intensity variation as a function of time $I_{bg}(t)$ is measured by the photodiode detector during sensor setup with no absorber present in the laser line-of-sight (LOS). The simultaneous wavelength modulation and scan for a single scan can be described as:

$$v(t) = \bar{v} + a \cos(2\pi ft + \varphi_v) + F(t), \tag{1}$$

where \bar{v} is the laser frequency (or wavelength) without injection-current tuning, $a[\text{cm}^{-1}]$ the modulation depth, φ_v the phase of the frequency modulation and $F(t)$ the function describing the wide near-linear wavelength scan, normally

a polynomial of three to four orders. The absorption of the time-varying intensity is described by Beer-Lambert's law, and the simulated transmitted laser intensity $^S I_t(t)$ can be expressed as:

$$^S I_t(t) = I_{bg}(t) \cdot \exp[-\alpha(v(t))], \tag{2}$$

where $\alpha(v(t))$ is written:

$$\alpha(v(t)) = \exp\left(-\sum_j S_j \cdot \phi_j(v(t)) \cdot P \cdot x_i \cdot L\right). \tag{3}$$

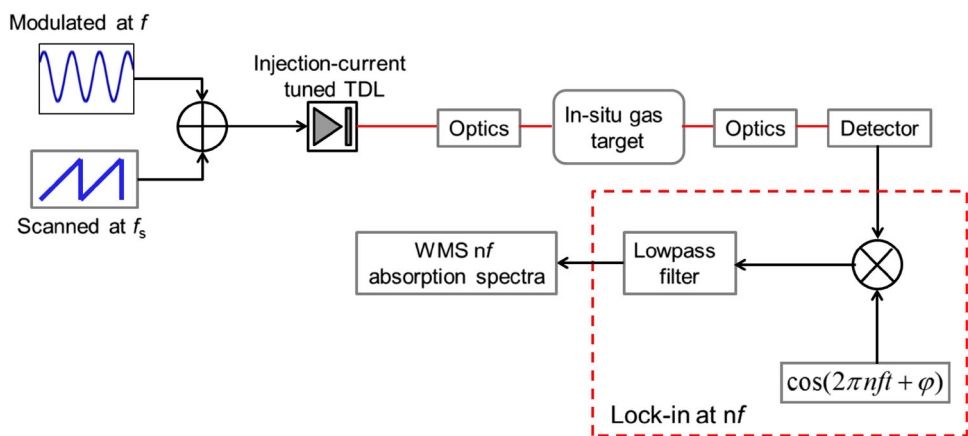
Here, S_j and ϕ_j are the linestrength and lineshape function of transition j , P the total pressure of the gas, x_i the mole fraction of absorber i and L the pathlength. Equation 3 assumes a uniform gas mixture and temperature along the LOS; for the gasifier application discussed below, the LOS is limited by the diameter of the confining pipe and the long flow distances assure good mixing. The product of $S_j \cdot P \cdot x_i \cdot L$ is defined as the absorbance area or the integrated absorbance. For known pressure, temperature, and pathlength, the absorber mole fraction can be determined from the absorbance area if the linestrength is known.

The Voigt lineshape [32] of a relatively isolated absorption transition is used here and is given by the convolution of a Doppler-broadening component (Gaussian) and a collisional-broadening component (Lorentzian); Δv_c is the full width at half maximum of the Lorentzian contribution to the Voigt. In the limit of binary collisions, the width is proportional to pressure at constant temperature, and for a multi-component gas mixture, the total collisional width can be obtained by summing the contributions from all components:

$$\Delta v_c = 2 \cdot P \cdot \sum_j x_j \cdot \gamma_j(T) \tag{4}$$

where x_j is the mole fraction of species j , and γ_j is the broadening coefficient due to collisions by the j th species. The relationship between γ_j and T can be described as:

Fig. 1 Schematic of the experimental setup of a typical WMS measurement and approaches to obtain the WMS-*nf* absorption spectra



$$\gamma_j(T) = \gamma_j^{296\text{K}} \cdot \left(\frac{296}{T}\right)^{n_j} \quad (5)$$

where n_j is the temperature exponent of the collisional-broadening coefficient.

A digital lock-in is used to shift the nf harmonic components from nf frequency to zero frequency, by multiplying the simulated ($^S I_i(t)$) and measured ($^M I_i(t)$) transmitted laser intensities by $\cos(n \cdot 2\pi ft)$ for the X component (real) and $\sin(n \cdot 2\pi ft)$ for the Y component (imaginary). A numerical low-pass filter with a bandwidth less than $f/2$ is then used to extract these components:

$$X_{nf} : I_i(t) \cdot \cos(n \cdot 2\pi ft) \rightarrow \text{lowpass filter.} \quad (6)$$

$$Y_{nf} : I_i(t) \cdot \sin(n \cdot 2\pi ft) \rightarrow \text{lowpass filter.} \quad (7)$$

The absolute magnitude of the WMS- nf signal is then given as:

$$S_{nf} = \sqrt{X_{nf}^2 + Y_{nf}^2}. \quad (8)$$

To account for time-varying non-absorption transmission losses, the $1f$ signal can be used to normalize the nf signal:

$$S_{nf\text{normalized}} = S_{nf}/S_{1f} \quad (9)$$

Analogous to wavelength-scanned DA, the integrated absorbance area (or the absorber mole fraction if the line-strength, pressure, temperature and pathlength are known) and the collisional width of the transition can be varied to achieve the best fit between the simulation and the measurement for each normalized WMS- nf absorption spectrum.

3 Laboratory test of sensor performance

Because the gasifier measurements were the first application of the wavelength-scanned WMS method [26, 27] at increased pressures, laboratory measurements at known conditions were conducted from 3 to 15.8 atm. A transition near $7,393.84 \text{ cm}^{-1}$ [(1, 0, 1) \leftarrow (0, 0, 0) $\nu' \leftarrow \nu''$ and (9, 1, 9) \leftarrow (8, 1, 8) rational level with a lower state energy, $E'' \sim 744 \text{ cm}^{-1}$] was selected to probe H_2O mole fraction in the gasifier output (see Fig. 2). The absorption feature is in fact two closely spaced transitions with the same E'' positioned at $7,393.79$ and

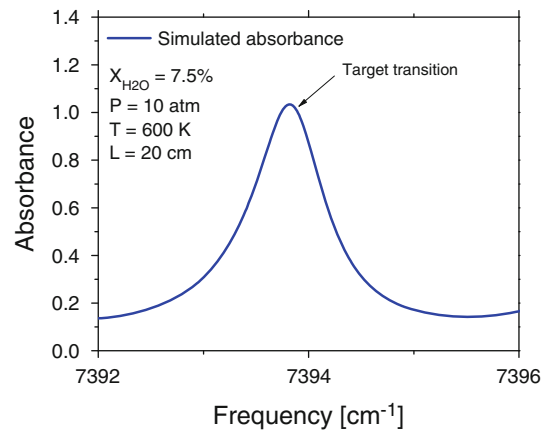


Fig. 2 Simulated absorption spectrum for H_2O molecule at typical gasifier conditions

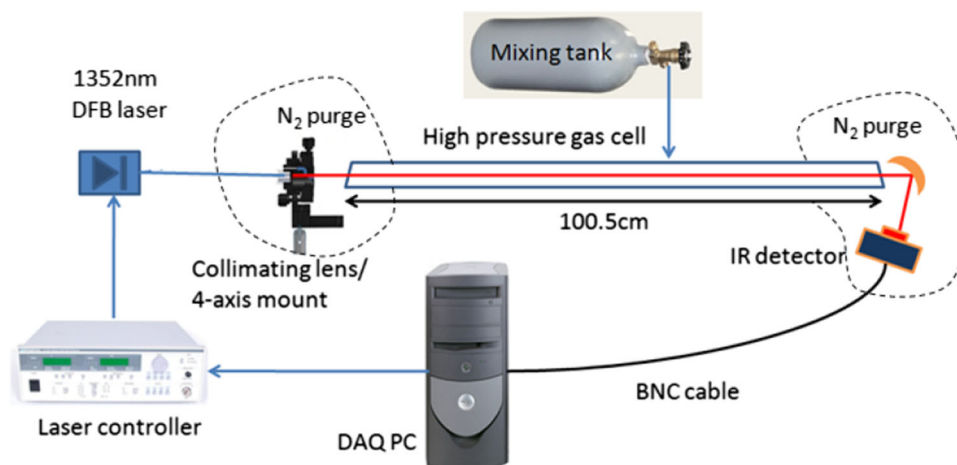
$7,393.84 \text{ cm}^{-1}$. The laboratory-measured spectroscopic data [29] and HITRAN database [33] suggest that at high pressure, this line pair can be considered as a single transition with one set of line-broadening parameters. The spectroscopic data used here for this transition are listed in Table 1. This transition pair was selected for four reasons: (1) the absorption is strong at the measurement temperature (near 600 K), providing good signal-to-noise ratio in gasifier environment; (2) the transition is well isolated from neighbors at increased pressures; (3) the $2f/1f$ absorption signal is not sensitive to temperature changes in the region near 600 K; and (4) the collisional width is small, providing narrow lineshape to enhance WMS signals. Note that here and throughout the paper the SNR is defined as the ratio of the $1f$ -normalized WMS- $2f$ peak signal to the standard deviation of the residuals from the WMS model fit.

To test the H_2O sensor in the laboratory, absorption near $7,394.8 \text{ cm}^{-1}$ was measured for a known H_2O mole fraction in a 100.5-cm-long cell at room temperature at pressures ranging from 3 to 15.8 atm (Fig. 3). The cell was first evacuated to measure a background signal, then filled with $\text{H}_2\text{O}/\text{Air}$ mixture at constant pressure. The mixture was premixed and stored overnight to ensure homogeneity. A DFB laser (NEL) near $1,352 \text{ nm}$ with single-mode fiber output was injection-current modulated with a sine function at 10 kHz, superposed on a

Table 1 Laboratory measured spectroscopic parameters [linestrength, collisional-broadening coefficients and their temperature dependence exponents (in the parentheses)] at 296 K for the target transition using the procedure from Ref. 32

Linecenter (cm^{-1})	Linestrength ($\text{cm}^{-2} \text{ atm}^{-1}$)	Lower state energy (cm^{-1})	$2\gamma_{\text{H}_2\text{O}-\text{H}_2\text{O}}$ ($\text{cm}^{-1} \text{ atm}^{-1}$) ($n_{\text{H}_2\text{O}-\text{H}_2\text{O}}$)	$2\gamma_{\text{H}_2\text{O}-\text{CO}_2}$ ($\text{cm}^{-1} \text{ atm}^{-1}$) ($n_{\text{H}_2\text{O}-\text{CO}_2}$)	$2\gamma_{\text{H}_2\text{O}-\text{CO}}$ ($\text{cm}^{-1} \text{ atm}^{-1}$) ($n_{\text{H}_2\text{O}-\text{CO}}$)	$2\gamma_{\text{H}_2\text{O}-\text{N}_2}$ ($\text{cm}^{-1} \text{ atm}^{-1}$) ($n_{\text{H}_2\text{O}-\text{N}_2}$)	$2\gamma_{\text{H}_2\text{O}-\text{H}_2}$ ($\text{cm}^{-1} \text{ atm}^{-1}$) ($n_{\text{H}_2\text{O}-\text{H}_2}$)
7,393.84	0.0690	744	0.530 (0.650)	0.139 (0.957)	0.119 (0.620)	0.088 (0.575)	0.082 (0.463)

Fig. 3 Laboratory measurement setup for validation of the wavelength-scanned WMS strategy for high-pressure gas sensing



sawtooth function at 25 Hz using computer-driven outputs (National Instruments PCI-6115 and ILX Lightwave LD-3900). After collimation, the laser beam travelled through the cell and was focused onto a NIR photodiode detector (Thorlabs PDA-10CS). The voltage signal on the gain-adjustable detector was then sampled (National Instrument, PCI-6115, 12 bit, ac-coupled) and numerically post-processed with a lock-in digital finite-impulse response (FIR) low-pass filter bandwidth of 2 kHz. The line-of-sight (LOS) pathlength external to the cell was purged by pure N_2 gas to minimize absorption from ambient atmospheric water vapor.

Figure 4 shows the measured $1f$ -normalized WMS- $2f$ spectrum at three different modulation depths as well as the best-fit results at known conditions of $P = 10$ atm, $T = 296$ K. The calibrated H_2O water vapor mole fraction in the mixture was 0.00096 and the expected FWHM collisional width is 0.81 cm^{-1} ($2\gamma_{H_2O-Air} = 0.081 \text{ cm}^{-1}/\text{atm}$, determined by DA measurements at sub-atmosphere pressures). The WMS analysis procedures in Refs. [26] and [27] include the laser intensity modulation (to all orders), and we speculate the remaining differences in Fig. 4 result from imprecision of the spectral model, with two likely reasons: (1) The lineshape at high pressures can be non-Voigt due to line mixing and other phenomena. (2) The signal can include contributions from collision broadening of less well-characterized neighboring transitions, which can be more significant in the wings of the lineshape. Nevertheless, the overall comparison reveals better than 2% agreement in the known H_2O mole fraction, demonstrating the feasibility of using the $1f$ -normalized wavelength-scanned WMS- $2f$ strategy for simultaneous determination of absorber mole fraction and collisional width of the transition at high pressures.

Figure 5 presents the collisional widths, integrated absorbance and the resulting H_2O mole fractions that best

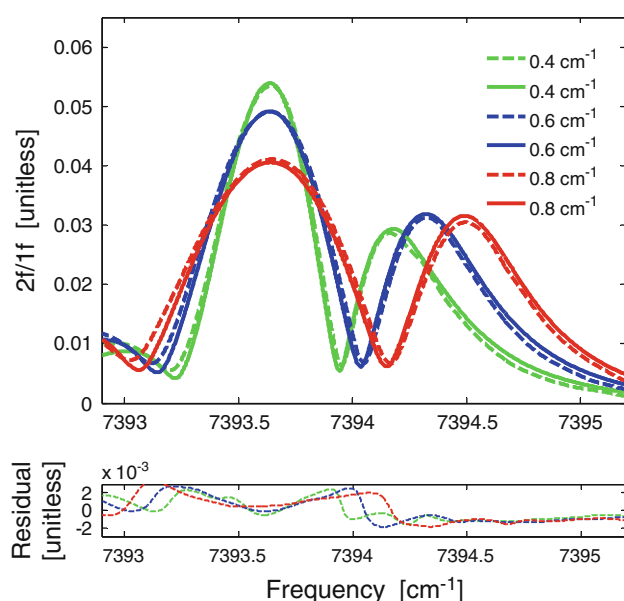


Fig. 4 Measured (solid lines) single-sweep WMS- $2f/1f$ lineshape using different modulation depths and the best-fit results (dashed lines) (best-fit parameters: for $a = 0.4 \text{ cm}^{-1}$, $x_{H_2O} = 0.000953$, $\Delta\nu_c = 0.823 \text{ cm}^{-1}$, for $a = 0.6 \text{ cm}^{-1}$, $x_{H_2O} = 0.000947$, $\Delta\nu_c = 0.820 \text{ cm}^{-1}$, for $a = 0.8 \text{ cm}^{-1}$, $x_{H_2O} = 0.000961$, $\Delta\nu_c = 0.802 \text{ cm}^{-1}$). Lower panel shows the residuals of the fit

fit the measured WMS absorption spectra at pressures ranging from 3.2 to 15.8 atm, measured with a modulation depth of 0.8 cm^{-1} . The small deviation (<2%) between the measurements and the expected values indicates as follows: (1) the fitting strategy for wavelength-scanned WMS simultaneously yields the transition-integrated absorbance and collisional width, even at high pressures up to 15.8 atm; (2) the non-ideal Lorentzian behavior, such as line mixing and the finite-collision breakdown do not have significant influence on determining the mole fraction for this target transition and this range of conditions.

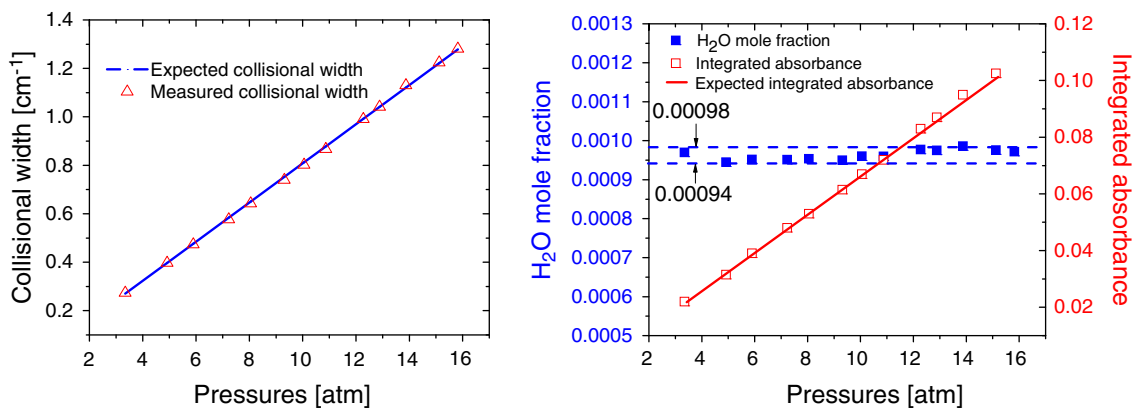


Fig. 5 Best-fit results for the transition collisional width (*left panel*) and integrated absorbance and mole fraction (*right panel*) with comparisons to the expected values at different pressures ($T = 296$ K, $L = 100.5$ cm)

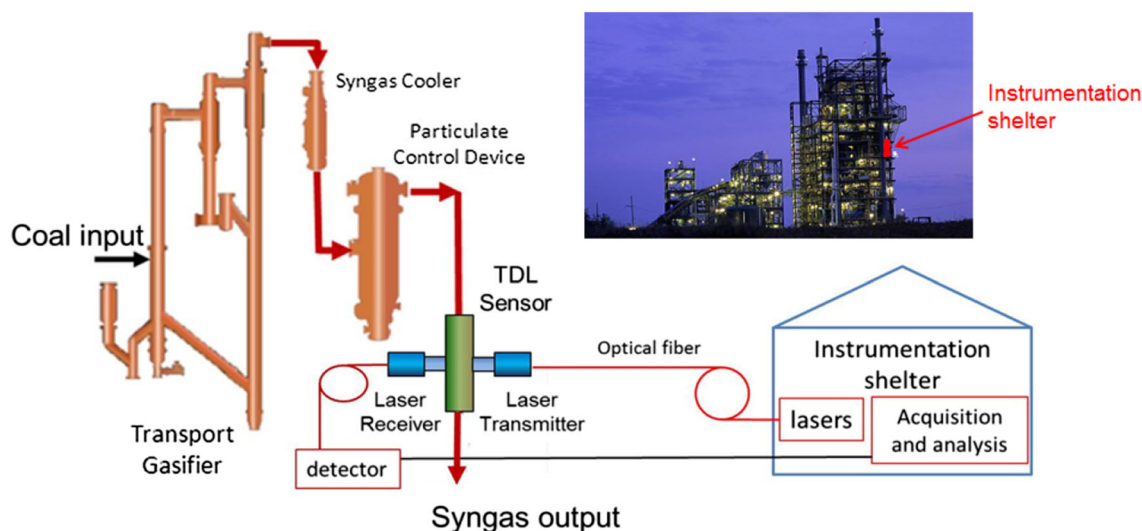


Fig. 6 Location of the TDL sensor in the syngas process piping 30 meters downstream of the exit of the PCD. Note the lasers and supporting electronics were remotely located in the instrumentation shelter

4 Field measurement campaign

4.1 Gasifier facility and measurement setup

The laser sensor performance was evaluated in an engineering-scale transport reactor gasifier at the National Carbon Capture Center operated for US Department of Energy by Southern Company Services in Wilsonville Alabama, USA[31]. Optical access was selected 30 m downstream from the exit of the particulate control device (PCD) of the gasifier, with the laser transmitter and receiver optics located on either side of the syngas output pipe, as illustrated in Fig. 6, and typical conditions are listed in Table 2.

Table 2 Typical conditions at the measurement location

Property	Values
Temperature (K)	600
Pressure (atm)	15
Pathlength (cm)	20
H ₂ O mole fraction	0.06–0.10
CO ₂ mole fraction	0.06–0.10
CO mole fraction	0.08–0.12
H ₂ mole fraction	0.06–0.10
Trace species mole fraction (H ₂ S, NH ₃ , etc.)	<0.01
Flow rate (kg/h)	12,500

The gas mixture is balanced by N₂

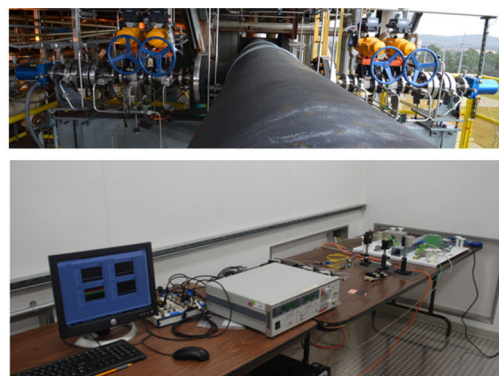
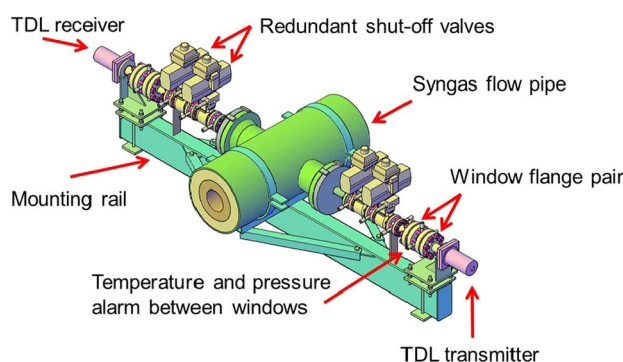


Fig. 7 Schematic (*left*) and photograph (*right upper*) of the sensor installation showing the mounting rail hanging on the syngas pipe with redundant actuated shutoff valves, redundant window pairs,

The optical access was designed to insure safe containment of the toxic and explosive syngas (high concentrations of CO and H₂) in the event of a window failure, as illustrated in the schematic of Fig. 7. A pair of flange-mounted sapphire windows was installed on either side of the rig, and measurement of temperature and pressure between the windows provided a safety alarm in the event of window failure. Such a failure would trigger automatic closing of the valves on both the transmitter and receiver optics (thereby avoiding fugitive syngas emission). The transmitter and receiver packages for the laser and detector optics were enclosed in purged metal cans and the optics were remotely adjusted to optimize sensor alignment using low-voltage DC motors. Laser light was produced in the instrumentation shelter and coupled to the transmitter via optical fiber, and the transmitted light was collected and delivered via optical fiber to a detector located nearby (~ 2 m) in a small purged enclosure that meets the explosion proof NEMA (National Electrical Manufacturers Association) standards for this industrial application. The light was detected on a low-voltage DC detector and the DC signal returned to the instrument shelter for processing.

The zero-absorption transmitted laser intensity, $I_{bg}(t)$, was determined using two different strategies. (1) The zero-absorption laser intensity was measured in the laboratory (at Stanford) using the laser transmitter and receiver optics and the four window flanges. (2) When the instrument was installed in the field, there was an opportunity to measure the zero-absorption transmitted intensity of the sensor with the gasifier filled with nitrogen. These two methods returned nearly identical WMS- $2f$ background signals. In addition, the WMS background was quite small compared to the WMS signal ($< 2\%$), which is a value similar to the fit residuals, and the WMS background could have been neglected in this high-absorbance application without significant change in the results. Any window fouling or overall transmission losses (e.g., scattering

temperature and pressure alarm for window failure, and the TDL transmitter and receiver housings. The TDL electronics in the shelter are shown in the *right bottom panel*

losses) were accounted for in the measurement scheme by the $1f$ -normalization. The scattering losses were observed to change with large changes in operating parameters (e.g., reactor pressure), but these changes were relatively slow ($\ll 10$ kHz) and did not affect sensor performance.

4.2 Measurement results

The wavelength-scanned WMS strategy as validated by the laboratory measurements was used to continuously monitor the water vapor content in the syngas product flow at different gasifier operation conditions. The facility operation began by igniting a propane/air burner in the reactor. When the reactor was hot enough, pulverized coal was added into the reactor to first initiate coal combustion and then begin the gasification process. The coal-fuel feeding continued for more than 10 h for this 1st start-up attempt, but was terminated at hour 52 to correct a problem elsewhere in the gasifier.

The water vapor level recorded for hours 0–52 with 2-s time resolution is shown in Fig. 8 (although the scan rate was 25 Hz, one scan of data was collected every 2 s to reduce computational and data storage requirements). During the gasification measurements, the transmitted laser intensity produced a signal of ~ 0.1 V (Thorlabs PDA 10CS detector with 30 dB gain) using a full-scale DAQ input range of -0.2 to 0.2 V. Thus, the one-bit resolution was 9.8×10^{-5} V, more than 100 times smaller than the peak $2f$ signal of ~ 0.01 V.

The water vapor mole fraction was inferred by fitting the measured $1f$ -normalized wavelength-scanned WMS- $2f$ single-sweep lineshape using two free parameters: the absorber mole fraction and the collisional contribution to the Voigt linewidth; the temperature and thus the Doppler contribution to the Voigt linewidth is known. Examples of a single-sweep fit and the residual differences to the lineshape fit are shown in Fig. 9. Due to the severe

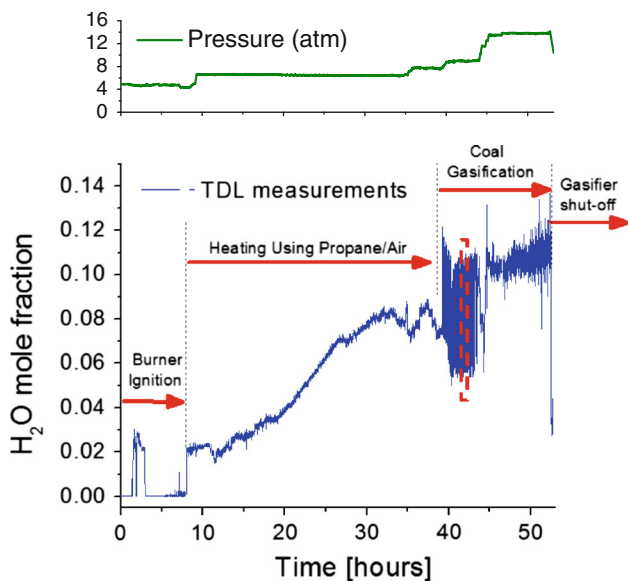


Fig. 8 In situ measurements of exhaust gas water vapor during reactor start-up including ignition of the propane burner, switch to coal combustion with pulsed coal feed, transition to gasification, and reactor shut down when the coal input was terminated. The pressure trace was provided by NCCC. The region surrounded by the *red dashed rectangle* is shown in Fig. 10. Note residuals to the H_2O mole fraction from the fit to the WMS scan are not observable on the scale of this plot (see Fig. 10)

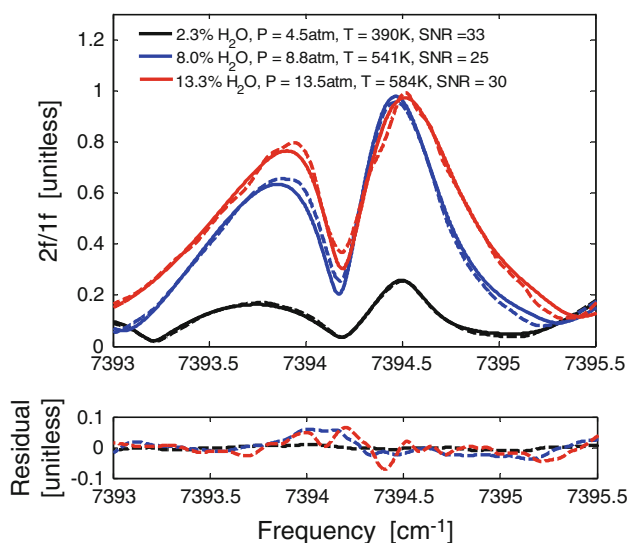


Fig. 9 Measured (*dashed line*) WMS- $2f/1f$ absorption spectra and the best-fit results (*solid lines*) at different gasifier operation conditions (*black*: heating using the propane/air flame, *blue*: coal combustion, *red*: coal gasification). $f_s = 25$ Hz, $f = 10$ kHz, $a = 0.78$ cm $^{-1}$. Pressure and temperature data were provided by NCCC

transmission losses due to beam steering and particulate scattering, the fractional light transmission was typically less than 10^{-4} . The SNR does not significantly vary as the reactor transitioned from combustion heating to

gasification, and we speculate this has two underlying causes: (1) Although light transmission was reduced and pressure was higher during gasification, the H_2O mole fraction and number density (thus the absorption signal) were significantly larger during gasification. (2) The $1f$ -normalized WMS- $2f$ signal is nearly unaffected by the attenuation of the light transmission. The signal-to-noise ratio was >20 for measurement period after the burner was ignited at hour 8.

From hour 0–4, several attempts to ignite the reactor burner were made, but the propane/air flame was unstable. This abnormal process was captured by TDL measurements as the H_2O mole fraction spiked and dropped rapidly several times during this period. At hour 8, a stable propane flame was established and the warm-up period began. The water vapor content of the syngas steadily increased at the measurement location during warm-up; this variation was expected as the fuel/air ratio of the propane burner was increased and as the output gas piping warmed to eliminate condensation.

At hour 38, propane heating ceased and the coal feeding began. The large fluctuations in H_2O mole fraction during the gasification were not caused by signal noise but by variations in the coal feed rate. Two factors support this conclusion: (1) The independent measurement by the reactor thermocouple were correlated with TDL water vapor measurements, as seen in the left panel of Fig. 10; (2) as shown in the right panel, the measured WMS- $2f/1f$ lineshapes were free of noise and the increase in absorption at measurement time point 2 was obviously larger than the one at point 1, indicating more H_2O molecules in the laser line-of-sight. This water vapor variation corresponded to the pulsing of the coal feed rate to slow the warm-up rate of the facility and prevent damage to the ceramic lining of the gasifier and the output plumbing. With the 2-s time resolution, the TDL sensor captures the time-varying water vapor in the exhaust gas due to the changing fuel content in the reactor. Such results were not found in the GC measurement results (5 min time resolution) made downstream for sampled CO_2 . This demonstrates the advantage of in situ TDL measurement over sampled GC measurements for time-resolved monitoring of the gasifier performance during start-up. Surprisingly, the SNR was smaller at the larger values of H_2O mole fraction. We speculate that the $1f$ signal used for normalization distorted the signal at large absorbance increasing the uncertainty in the fit.

Figure 11 shows the measured collisional width after the burner was ignited and the comparison to expected results. The expected collisional width was based on the GC gas composition results, the TDL measured water vapor mole fraction and the broadening coefficients pre-measured in the laboratory using equations (4) and (5). The comparison

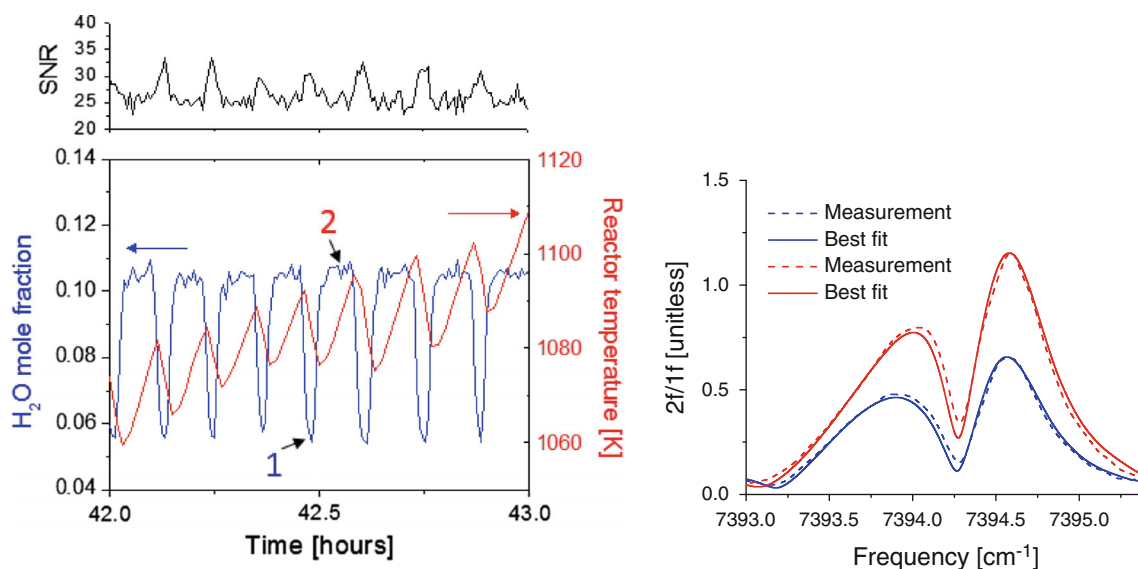


Fig. 10 *Left panel:* TDL sensor measured water vapor mole fraction from hour 42 to hour 43 and the reactor temperature measured by the thermocouple; *Right panel:* measured WMS-2f/1f absorption spectra

at point 1 (the lowest water vapor mole fraction in a single pulse) and at point 2 (the highest water vapor mole fraction in a single pulse). The SNR versus time is shown in the *upper left panel*

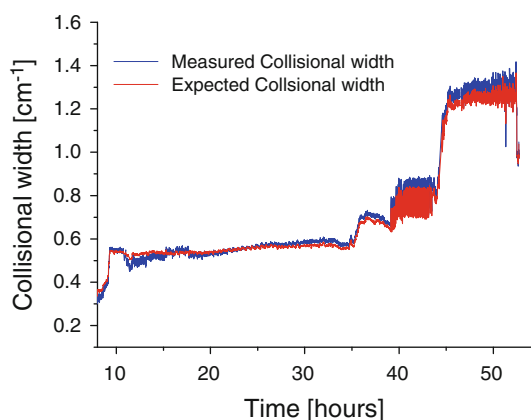


Fig. 11 TDL sensor measured transition collisional width and its comparison to the expected values

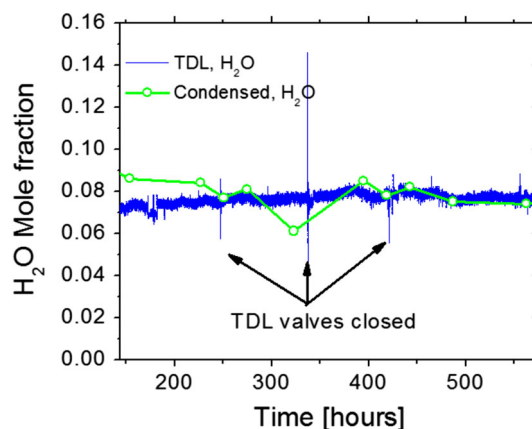


Fig. 12 TDL sensor recorded water vapor content in the syngas without people attendance for a duration of more than 400 h

revealed better than 3 % agreement, which was perhaps fortuitous as the combined uncertainty in gas composition (from GC measurements), and the database of collisional-broadening coefficients was in excess of this value. Note the variations in the collisional width measurements from hour 40–52 correlated with the water vapor mole fraction variation due to changes in the coal feed rate, as H₂O is a much more effective collision partner for collisional broadening than other components of the syngas (see Table 1). The agreement between values and the time variation of the modeled collision-broadened linewidth and fit values of the collision-broadened linewidth provides confidence that the wavelength-scanned WMS data analysis scheme [26, 27] can be used without prior knowledge

of the transition collisional width, even at the increased pressures of ~ 15 atm. Thus, a practical sensor can be quantitatively analyzed without calculating or estimating the expected collisional width, thereby avoiding the assembly of a collisional-broadening database and a reasonably accurate estimate (or in this case GC measurement) of the gas composition.

The TDL water vapor sensor operated unattended from hour 140 until hour 575, and continuous records of H₂O and temperature were collected except for three short (~ 10 min) periods when the valves on the optical access were closed due to independent gasifier upsets. During the entire period, the transmission of the TDL sensor remained stable (transmission $\geq 3 \times 10^{-5}$), and the windows did

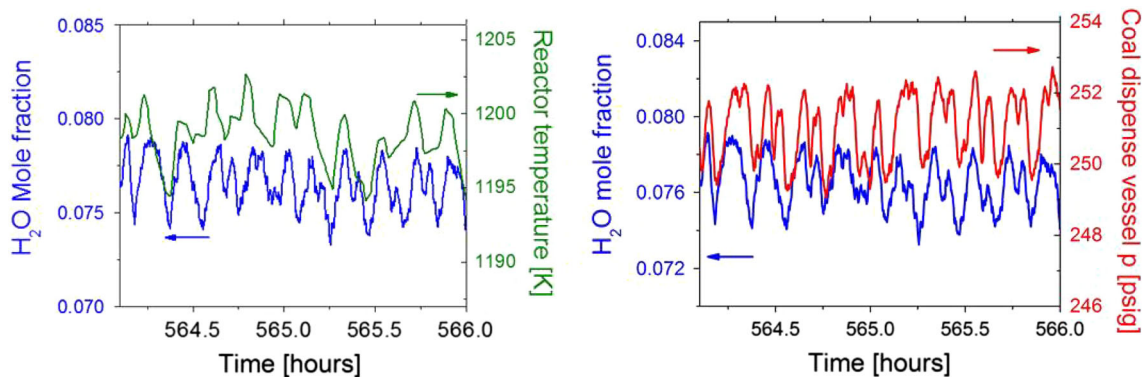


Fig. 13 Correlations of the TDL sensor measured water vapor content in the syngas product flow with the reactor temperature measured by a thermocouple (*left*) and the coal-dispense vessel pressure (*right*)

not exhibit any indications of fouling. The syngas water vapor record is illustrated in Fig. 12 and compared with samples of liquid water extracted from the syngas stream. These two H₂O measurement methods have similar mean values over the 435 h record, with larger variations seen in the liquid water sampling.

Evaluating the accuracy and the precision of the TDL sensor measurements is not straightforward. The facility is not equipped with an accurate water vapor measurement for calibration. The residuals to the fits to single-sweep waveforms as shown in Figs. 9 and 10, suggest an accuracy of a few percent (consistent with the small differences between measured and calculated line-widths), but without an accurate calibration the sensor accuracy can only be speculated. However, there is significant evidence the TDL sensor measured H₂O mole fraction has quite good (relative) precision. The H₂O mole fraction data of Fig. 12 vary with time by approximately ± 0.002 , which might suggest that the TDL sensor has a $\pm 3\%$ statistical uncertainty. However, there is a compelling argument that this fluctuation is a real change in the H₂O mole fraction. When the data are examined on a more expanded timescale, the measured mole fraction has a distinct oscillation (period of ~ 10 min) as illustrated in Fig. 13. These oscillations in H₂O are strongly correlated with the reactor temperature (left panel) and the coal-dispense vessel pressure (right panel). As this pressure increases so does the coal feed rate assuming constant reactor pressure. NCCC engineers speculated that the variations of the water vapor content are due to coal feed rate oscillations, which would produce small changes in the reactor fuel/air equivalence ratio and thus the amount of product H₂O. It is notable that these fluctuations were first observed by in situ TDL measurements. These facts suggest the relative measurement precision in the water vapor mole fraction is $\leq 1\%$.

5 Conclusions

A 1,352 nm DFB laser-based H₂O absorption sensor employing a $1f$ -normalized, wavelength-scanned WMS- $2f$ technique was developed for use in the high-pressure synthesis gas from an engineering-scale coal gasifier. The performance was first evaluated in the laboratory for pressures from 3 to 15.8 atm. The SNR was better than 30 for measurements of 0.023 mol fraction of H₂O at 25 Hz, corresponding to a ~ 800 ppm detection limit for water vapor mole fraction for a 25 Hz bandwidth. The sensor was then successfully applied to monitor the syngas output from an engineering-scale transport reactor coal gasifier at the National Carbon Capture Center. The gasifier pressures ranged up to 15 atm (~ 220 psig) and temperatures up to 650 K. Continuous monitoring of water vapor level in the gasifier output with 2-s time resolution was performed by the TDL sensor for more than 500 h, including the periods of burner ignition, combustion heating with a propane flame, coal combustion, coal gasification and reactor shut down via coal feed termination. As expected for coal syngas applications, beam steering and particulate scattering were severe during the measurements, resulting in less than 10^{-4} light transmission. With 2-s time resolution, the TDL sensor captured the time-varying changes in the water vapor level in the gas exhaust that could be correlated with the changing fuel content in the reactor. The variation of H₂O in the syngas due to the batch feeding of coal had been anticipated, but was observed for the first time by the TDL sensor as the GC analysis of the syngas sampled from the facility did not have the time resolution needed to observe this behavior. These facts strongly suggest that the observed fluctuations in the gas composition observed by the TDL sensor were fluctuations in the gas composition, and thus the relative measurement errors in the water vapor mole fraction were smaller than 1% (these small variations were less than other relative or absolute syngas

composition data available for comparison). These results demonstrate the feasibility of using TDL sensors to provide real-time control signals to optimize the gasification.

A novel method of WMS analysis enabled the $1f$ -normalized, wavelength-scanned WMS- $2f$ measurements to determine the collisional width of the target transition via lineshape fitting. Comparisons between the measured results and the expected values provided better than 3 % agreement (this is perhaps fortuitously good given the uncertainty of the GC measurements of the synthesis gas composition and the collision-broadening-coefficient database). The agreement of measured and modeled transition linewidth suggest that wavelength-scanned WMS can be used, similar to scanned-wavelength direct absorption, to determine the absorber mole fraction without knowledge of the transition collisional width prior to the measurement. This is important for ensuring accuracy of the measurements, as for many applications the gas composition can be difficult to estimate, and the uncertainty in estimating the transition collisional width can result in large errors in determining the absorber mole fractions via traditional analysis of WMS. This successful demonstration of water vapor measurement in the syngas output of a large-scale industrial facility shows advantages of using wavelength-scanned WMS techniques. Based on these successful H₂O measurements, future work will include extended wavelength-scanned WMS TDL sensors for other major species in the syngas output such as CO.

Acknowledgments The Stanford research was supported by the Electric Power Research Institute with Mr. Jose Marasigan as technical monitor and by US Department of Energy NETL with Dr. Susan Maley as technical monitor. The operation of the NCCC by Southern Company Services was supported by DoE.

References

1. T.F. Wall, Proc. Comb. Inst. **31**, 31 (2007)
2. S.J. Clayton, G.J. Stiegel, J.G. Wimer, US DoE report DOE/FE-0447 (2002)
3. R.K. Hanson, Proc. Combust. Inst. **33**, 1 (2011)
4. O. Axner, P. Kluczynski, A.M. Lindberg, J. Quant. Spectrosc. Radiat. Transf. **68**, 299 (2009)
5. P. Kluczynski, A.M. Lindberg, O. Axner, J. Quant. Spectrosc. Radiat. Transf. **83**, 345 (2004)
6. G. Hancock, J.H. van Helden, R. Peverall, G.A.D. Ritchie, R.J. Walker, Appl. Phys. Lett. **94**, 201110 (2009)
7. J.A. Silver, Appl. Opt. **31**, 707 (1992)
8. X. Chao, J.B. Jeffries, R.K. Hanson, Meas. Sci. Technol. **20**, 115201 (2009)
9. R.T. Wainner, B.D. Green, M.G. Allen, M.A. White, J. Stafford-Evans, R. Naper, Appl. Phys. B **75**, 249 (2002)
10. J.A. Silver, D.J. Kane, Meas. Sci. Technol. **10**, 845 (1999)
11. T. Fernholz, H. Teichert, V. Ebert, Appl. Phys. B **75**, 229 (2002)
12. V. Ebert, K.-U. Pleban, J. Wolfrum, in *In situ Oxygen-Monitoring Using Near-Infrared Diode Lasers And Wavelength Modulation Spectroscopy*, OSA 1998 Technical Digest Series Vol 3: Laser Applications to Chemical and Environmental Analysis, paper LWB3 (1998)
13. I. Linnerud, P. Kaspersen, T. Jaeger, Appl. Phys. B **67**, 297 (1998)
14. S. Lundqvist, P. Kluczynski, in Process Analytical Applications in the Mid-Infrared, *Proceedings of the SPIE 7945, Quantum Sensing and Nanophotonic Devices VIII, 79450N* (January 24, 2011). doi:10.1117/12.871571
15. J. Wolfrum, Proc. Comb. Inst. **27**, 1 (1998)
16. R.R. Skaggs, R.G. Daniel, A.W. Miziolek, K.L. McNesby, C. Herud, W.R. Bolt, D. Horton, Appl. Spectrosc. **53**, 1143 (1999)
17. T. Gulluk, H.E. Wagner, Rev. Sci. Instrum. **68**, 230 (1997)
18. K. Sun, X. Chao, R. Sur, J.B. Jeffries, R.K. Hanson, App. Phys. B **110**, 497 (2013)
19. G.B. Rieker, X. Liu, H. Li, J.B. Jeffries, R.K. Hanson, Appl. Phys. B **87**, 169 (2007)
20. D.T. Cassidy, L.J. Bonnell, Appl. Opt. **27**, 2688 (1988)
21. D.T. Cassidy, J. Reid, Appl. Opt. **21**, 1185 (1982)
22. H. Li, G.B. Rieker, X. Liu, J.B. Jeffries, R.K. Hanson, Appl. Opt. **45**, 1052 (2006)
23. G.B. Rieker, J.B. Jeffries, R.K. Hanson, App. Phys. B **94**, 51 (2009)
24. X. Chao, J.B. Jeffries, R.K. Hanson, Appl. Phys. B **106**, 987 (2012)
25. X. Chao, J.B. Jeffries, R.K. Hanson, App. Phys. B **110**, 359 (2013)
26. K. Sun, X. Chao, R. Sur, C. Goldenstein, J.B. Jeffries, R.K. Hanson, Meas. Sci. Tech. **24**, 125203 (2013). doi:10.1088/0957-0233/24/12/125203
27. C.S. Goldenstein, C.L. Strand, I.A. Schultz, K. Sun, J.B. Jeffries, R.K. Hanson, Appl. Opt. **53**, 356 (2014)
28. K. Sun, R. Sur, X. Chao, J.B. Jeffries, R.K. Hanson, R.J. Pummill, K.J. Whitty, Proc. Comb. Inst. **34**, 3593 (2012)
29. R. Sur, K. Sun, J.B. Jeffries, R.K. Hanson, Appl. Phys. B **115**, 9 (2014)
30. R. Sur, K. Sun, J.B. Jeffries, R.K. Hanson, R.J. Pummill, T. Waind, D.R. Wagner, K. Whitty, Appl. Phys. B (2014). doi:10.1007/s00340-013-5644-6
31. <http://www.nationalcarboncapturecenter.com/>
32. A.B. Mclean, C.E.J. Mitchell, D.M. Swanston, J. Electron Spectrosc. **69**, 125 (1997)
33. L.S. Rothman, I.E. Gordon, Y. Babikov, A. Barbe, D. Chris-Benner, P.F. Bernath, M. Birk, L. Bizzocchi, V. Boudon, L.R. Brown, A. Campargue, K. Chance, E.A. Cohen, L.H. Coudert, V.M. Devi, B.J. Drouin, A. Fayt, J.-M. Flaud, R.R. Gamache, J.J. Harrison, J.-M. Hartmann, C. Hill, J.T. Hodges, D. Jacquemart, A. Jolly, J. Lamouroux, R.J. LeRoy, G. Li, D.A. Long, O.M. Lyulin, C.J. Mackie, S.T. Massie, S. Mikhailenko, H.S.P. Müller, O.V. Naumenko, A.V. Nikitin, J. Orphal, V. Perevalov, A. Perrin, E.R. Polovtseva, C. Richard, M.A.H. Smith, E. Starikova, K. Sung, S. Tashkun, J. Tennyson, G.C. Toon, V.I.G. Tyuterev, G. Wagner, The HITRAN2012 molecular spectroscopic database. J. Quant. Spectrosc. Radiat. Transf. **130**, 4–50 (2013)